Journal of Optoelectronics and Advanced Materials Vol. 2, March 2000, p. 65-72

STRUCTURAL INVESTIGATION OF A $La_{0.6}Y_{0.07}Ca_{0.33}MnO_3$ THIN FILM BY HIGH RESOLUTION TRANSMISSION ELECTRON MICROSCOPY

C. Ghica, L. C. Nistor, V. S. Teodorescu, M. Valeanu, C. Ristoscu[a], I. N. Mihailescu[a], J.-P. Deville[b], J. Werckmann[b]

National Institute of Materials Physics, PO Box MG 7, 76900, Bucharest-Magurele, Romania
[a]National Institute for Lasers, Plasmas and Radiation Physics, PO Box MG 54, 76900 Bucharest-Magurele, Romania
[b]Institut de Physique et Chimie des Matériaux de Strasbourg, 23 Rue du Loess, F-67037 Strasbourg Cedex, France

The morphology and structure of a $La_{0.6}Y_{0.07}Ca_{0.33}MnO_3$ thin film is studied by transmission electron microscopy. The film was grown by pulsed laser deposition (PLD) on an MgO-buffered silicon <100> wafer. The as-deposited films are polycrystalline and show a columnar morphology. We present a detailed high-resolution transmission electron microscopy structural study concerning a possible monoclinic distortion of the orthorhombic LYCMO crystal cell.

(Received February 22, 2000; accepted March 10, 2000)

Keywords: Pulsed laser deposition, Colossal magnetoresistance, High resolution transmission electron microscopy

1. Introduction

During the last decade, the interest of a large part of the international scientific community was captivated by the class of the so-called "colossal" magnetoresistive (CMR) materials. They belong to the perovskites family and have the general formula $LnAMnO_3$, where Ln represents a metal from the lanthanide group (La, Pr, Sm) and A a bivalent alkaline metal (Ca, Sr, Ba). Their importance is justified by the amplitude of the magnetoresistive effect they show, reaching up to 10^6 % in special temperature and magnetic field conditions, as reported in Ref. [1]. The interest for this class of materials is a double one:

-firstly, from the scientific fundamental point of view, there is not any physical model yet created to predict such high values of the CMR effect. Although the "double exchange" mechanism is known since 1951 [2], it can only describe qualitatively but no quantitatively the phenomenon. The quantitative aspect seems to be strongly influenced by the growth morphology (grain boundaries effects) [3], lattice strain (cell distortions) [4,5], chemical composition [6,7], etc.

-secondly, from the technological point of view, the huge amplitude of the MR effect recommends this class of materials as a serious candidate for the next generation of magnetic field sensitive materials used in manufacturing high capacity data storage supports or magnetic field sensors (hard-disk reading heads, for example).

We performed a conventional and high resolution transmission electron microscopy study (CTEM and HRTEM) on a $La_{0.6}Y_{0.07}Ca_{0.33}MnO_3$ (LYCMO) thin film obtained by pulsed laser deposition on a MgO buffered Si substrate. Thin films of manganite perovskite have already been deposited with excellent results onto MgO single crystal substrates [8-10]. Our study is mainly focused on the question concerning the exact crystalline structure of LYCMO in our samples. An important characteristic of the LCMO perovskitic structures is the specific stacking of the MnO_6

octahedra. It is generally accepted that they determine an orthorhombic structure with $a_0 \approx c_0 \approx a_p\sqrt{2}$ and $b_o \approx 2a_p$ (where a_p is the cell parameter in the perovskitic description) belonging to the Pnma space group There are two possible explanations for the specific features of experimental selected area electron diffraction HRTEM patterns along certain principal zone axes for LYCMO: a slight monoclinic distortion of the widely accepted orthorhombic cell could account for the presence of forbidden spots in the experimental SAED diffraction patterns and the corresponding effect in the HRTEM patterns [4,11]; on the other hand, little deviations from the perfect zone axis orientation of a LYCMO microcrystal could also generate the appearance of forbidden *0k0* reflections with $k=2n+1$ by non-linear interactions between the diffracted beams [12]. Using the EMS image simulating program we come to the conclusion that the monoclinic distortion can better explain our ED and HRTEM experimental patterns.

2. Experimental

Thin films have been deposited by laser ablation using a KrF^* excimer laser with a wavelength λ = 248 nm and a pulse duration $\tau_{FWHM} \approx$ 20 ns. The laser beam was focused onto the target by a convergent lens with 30 cm focal length, providing a laser fluency in the range of 2 - 2.5 J/cm^2. The deposition chamber was evacuated down to 10^{-4} Pa before filling it with oxygen as work gas. The experiments were performed in flowing oxygen atmosphere at 10 Pa in order to provide a fresh oxygen source all along the deposition. Stoichiometric $La_{0.6}Y_{0.07}Ca_{0.33}MnO_{3-\delta}$ targets have been prepared by solid state reaction from a mixture of metallic oxides La_2O_3, Y_2O_3, CaO and Mn_2O_3 heated at 900°C for 20 h. The reacted powder was sintered at 1200°C in ambient air into a pellet of 1.5 cm diameter which we used as target for the PLD experiments.

The target was mounted on a rotating table to avoid its piercing while the substrate was maintained at 750 °C during deposition. We used Si<100> wafers as substrates. Since the silicon is a semiconductor, in order to allow further magnetoresistance measurements on the LYCMO thin films we have firstly deposited an insulating MgO film as a buffer layer. After deposition, the sample was allowed to cool down slowly to the room temperature in a 10 mbar oxygen atmosphere.

The electron diffraction and transmission electron microscopy images were obtained on a Topcon EM 002B electron microscope operating at 200 kV with 0.18 nm point resolution.

A plane-view specimen was mechanically thinned from the substrate side down to about 15 μm using a Gatan dimple grinder. Electron transparency was achieved by ion milling in a Balzers installation. Also, a cross-section specimen was prepared by mechanical thinning in wedge shape down to electron transparency using the tripod method [13].

3. Results and discussion

3.1. CTEM results

The LYCMO as-deposited film is polycrystalline, as revealed by the micrograph taken on the plane-view specimen (Fig. 1). It shows a vague texturing tendency as indicated by the diffraction spots grouped into circular segments. The two pictures were obtained in a region where the specimen was thin enough so that they refer to the LYCMO film only, since there are no MgO diffraction rings in Fig. 1 b. The average LYCMO grain size is about 100 nm.

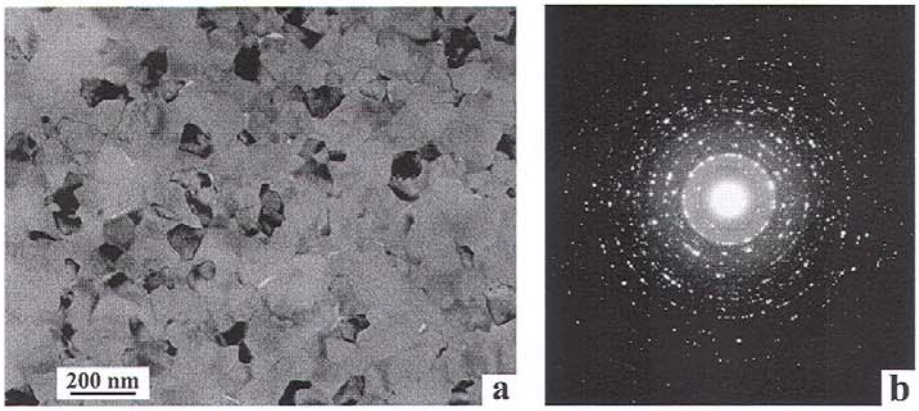

Fig. 1. Plane-view image (a) and the corresponding selected area electron diffraction pattern (b) obtained on the on-axis sample.

The cross-section image (Fig. 2) presents the LYCMO/MgO/Si sequence, with average thicknesses of about 190 nm and 120 nm corresponding to the LYCMO and MgO layers, respectively. Both films show columnar growth.

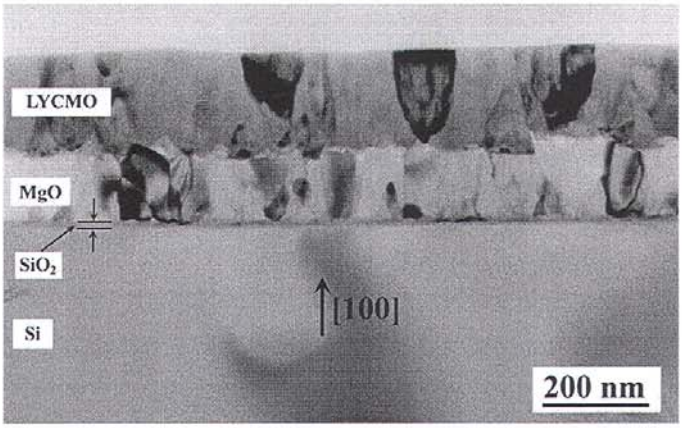

Fig. 2. Cross-section aspect of the on-axis LYCMO/MgO/Si sample.

The LYCMO - MgO interface is quite rough (up to 30 nm roughness) due to the faceted randomly oriented MgO columns. There is a 10 nm amorphous SiO_2 layer at the MgO - Si interface due to substrate high temperature during deposition in an oxygen atmosphere.

3.2 SAED and HRTEM study

Most of the authors associate the orthorhombic space group *Pnma* to the perovskitic magnetoresistive manganites. However, SAED and HRTEM patterns along certain zone axes cannot be correctly indexed or reproduced by the HRTEM image simulation programs using this space group. Recently, a slightly distorted, monoclinic unit cell has been proposed [4,12] in order to explain the presence of forbidden diffraction spots in the SAED patterns and the corresponding "doubling" of periodicity on the HRTEM micrographs. The following study comes to support the idea of a monoclinic cell, by presenting and analyzing some SAED and HRTEM patterns corresponding to a few principal zone axes.

Three diffraction patterns recorded on microcrystals in three different orientations are presented in Fig. 3 (a-c). The selecting area aperture was slightly larger than the chosen oriented microcrystals, including fragments of neighboring unoriented grains which introduced supplementary undesired diffraction spots. However, the diffraction patterns belonging to the well oriented grains

appear clearly enough and they were indexed according to the orthorhombic *Pnma* space group. As indicated by the question marks, beside the irregular undesired spots there are supplementary spots appearing in positions forbidden by the *Pnma* space group. Indeed, Miller indices of the allowed diffraction maxima must obey the following conditions, according to the *Pnma* selection rules:

0kl: k+l = 2n
hk0: h = 2n
h00: h = 2n
0k0: k = 2n
00l: l = 2n.

Or, as one can see, forbidden diffraction spots like 010_o and 001_o appear in the SAED patterns. The presence of forbidden reflections in the SAED patterns indicates a "doubling" of period in real space on the corresponding HRTEM images (Fig. 3 d-f). A 0.77 nm period instead of 0.385 nm is evident along $[010]_o$ (zone axes $[101]_o$ and $[001]_o$ in Fig. 10 a, b) and 0.54 nm instead of 0.27 nm along $[001]_o$ (zone axis $[-210]_o$ in Fig. 10 c). On the HR image presented in Fig. 3 f, the periodicity "doubling" occurs in one direction only out of the three disposed at 120° around the pseudo 6-fold symmetry zone axis **B** = $[-210]_o$. In fact, the microcrystal that this HR image belongs to, is made up of large domains where this periodicity doubling is unidirectional, only these special directions are rotated by 120° from one domain to another. Consequently, only one of the three forbidden spots (the closest to the central spot) should be explained.

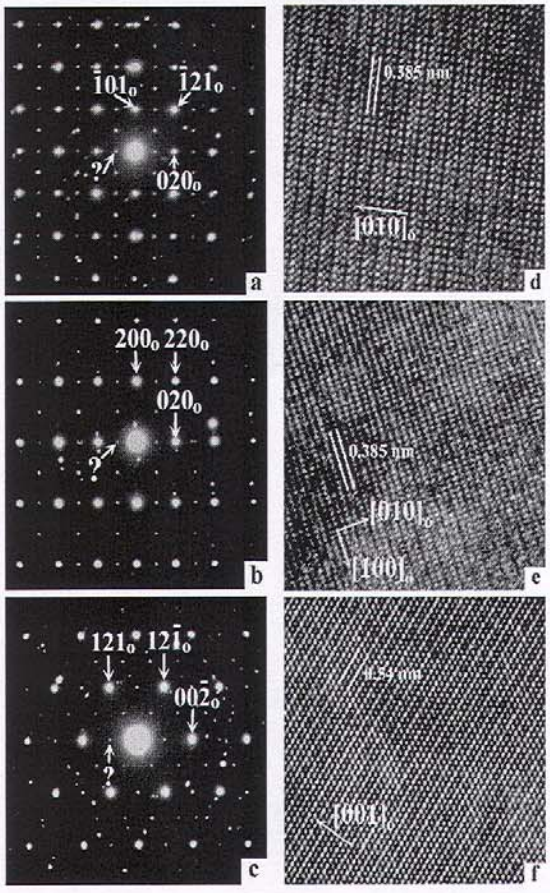

Fig. 3. SAED patterns (a-c) and the corresponding HRTEM images (d-f) in the case of three principal zone axes: $[101]_o$ in (a) and (d); $[001]_o$ in (b) and (e); $[-210]_o$ in (c) and (f); patterns are indexed according to the orthorhombic Pnma space group; interrogation marks indicate diffraction spots forbidden in Pnma; HRTEM images reveal a "doubled" period along $[010]_o$ (d and e) and $[001]_o$ (f).

Simulated HRTEM images (we used the EMS image simulating program) using *Pnma* as space group cannot reproduce the contrast obtained on the experimental micrographs. We give as an example a matrix of simulated HR images corresponding to **B** = $[101]_o$ zone axis, at various thicknesses and defocuses (Fig. 4). None of these simulated images can reproduce the "doubling" of periodicity along $[010]_o$ as revealed by the experimental micrographs.

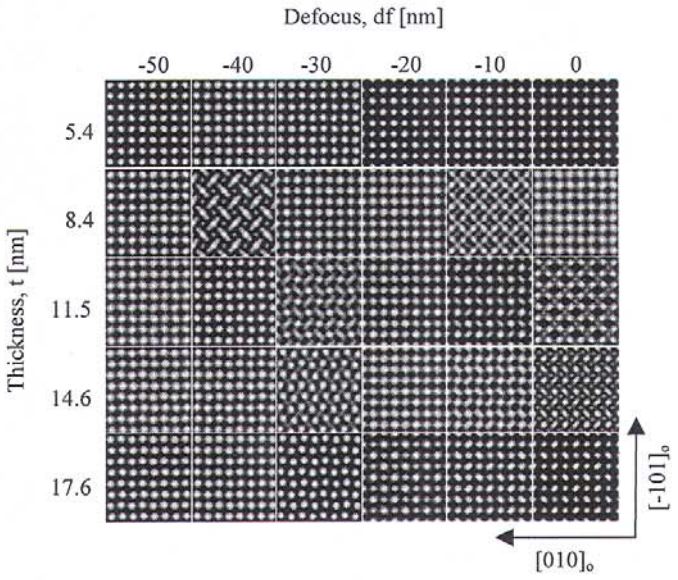

Fig. 4. Through-focus and through-thickness image series for **B** = $[101]_o$ using Pnma as space group.

The presence of supplementary diffraction spots and the resulting phase contrast could be explained by a monoclinically distorted lattice cell instead of the orthorhombic one. The presence of diffraction spots in $(010)_o$ positions suggests a structure with a lower symmetry obtained by removing the axial glide plane $a \perp [010]_o$. Consequently, for the lattice cell proposed to explain these features, the *a* glide plane has been eliminated by slightly shifting the O atoms in one out of two adjacent Mn-O layers so that these latter became parallel to $(010)_o$ lattice plans (Fig. 5). As a consequence, the concerned MnO_6 octahedra were slightly sheared and a little inclination was given to the lattice cell in order to obtain a monoclinic one. The new structure is described by the monoclinic $P2_1/c$ space group, a subgroup of *Pnma*, and the relation between the corresponding lattice unit vectors is:

$$a_m = b_o,\ b_m = c_o,\ c_m = a_o \text{ and } \beta_m = 90.3°.$$

The $P2_1/c$ reflection conditions:

$$h0l:\ l = 2n$$
$$0k0:\ k = 2n$$
$$00l:\ l = 2n$$

allow the presence of $100_m \equiv 010_o$ diffraction spots and the diffraction patterns corresponding to **B** = $[011]_m \equiv [101]_o$ and **B** = $[010]_m \equiv [001]_o$ (Fig. 3) can now be correctly indexed and completely explained. However, the $010_m \equiv 001_o$ reflection observed on the diffraction pattern in Fig. 3 c is not allowed by the $P2_1/c$ space group neither.

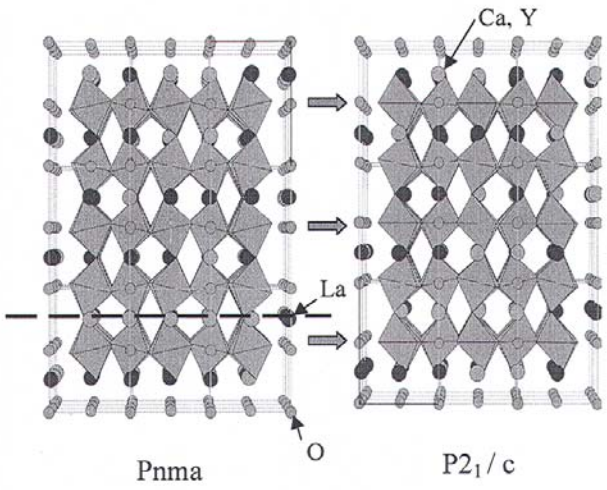

Fig. 5. Comparison between the Pnma and $P2_1/c$ structures presented as packed MnO_6 octahedra. Filled arrows indicate that one of two consecutive Mn-O plans were brought to horizontal position in order to eliminate the glide plan perpendicular to $[010]_o$.

Therefore, we consider that double diffraction could explain the presence of additional spots according to the schema presented in Fig. 6, where $-221_m \equiv 1\text{-}22_o$ and $4\text{-}1\text{-}2_m \equiv -2\text{-}14_o$ are allowed diffraction spots.

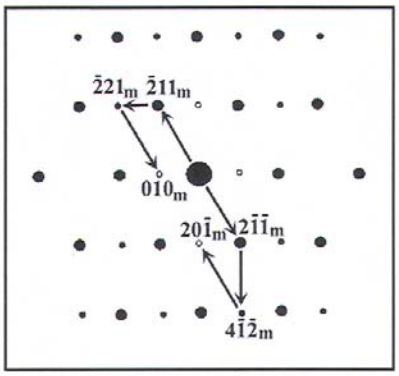

Fig. 6. Schema showing the double diffraction processes leading to additional spots in forbidden positions in the case of $\mathbf{B} = [102]_m \equiv [210]_o$ zone axis.

The pseudo 6-fold symmetry of the experimental diffraction pattern is obtained by superposing three such diffraction patterns rotated by 60° one to another, corresponding to single domains where the "double" periodicity is unidirectional.

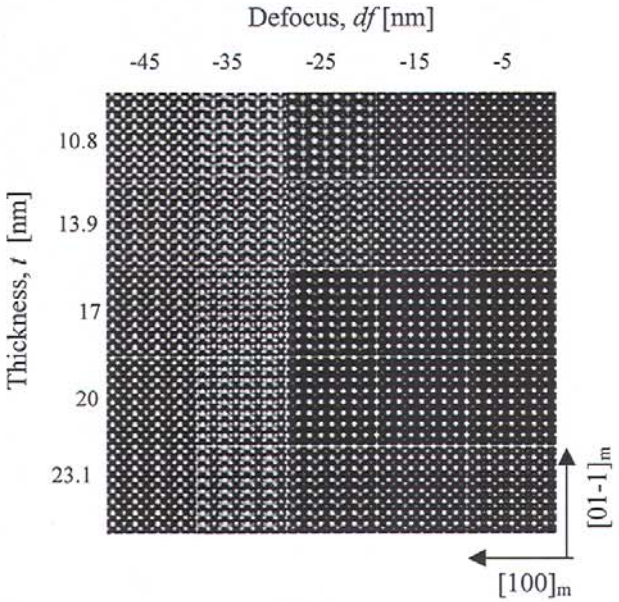

Fig. 7. Through-focus and through-thickness image series for $\mathbf{B} = [011]_m \equiv [101]_o$ using $P2_1/c$ as space group.

Moreover, simulated HR images obtained for the $P2_1/c$ space group can reproduce the "doubled" periodicity revealed by the experimental micrographs.

Fig. 7 shows a matrix of simulated HR patterns along $\mathbf{B} = [011]_m \equiv [101]_o$ using $P2_1/c$ as space group. The double periodicity along $[100]_m \equiv [010]_o$ is evident for all the simulated patterns. By comparing the simulated images with the experimental one, we consider that the latter coincides with the simulated pattern obtained for a defocus $df = -15$ *nm* and a thickness $t = 17$ *nm*. In order to illustrate the perfect HR contrast matching, the above mentioned simulated image has been superposed on the experimental micrograph (Fig. 8) in the right upper corner.

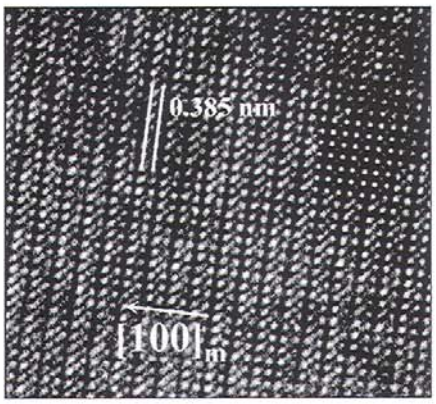

Fig. 8. Simulated HR image obtained for a thickness t = 17 nm and a defocus df = -15 nm has been superposed on the experimental HR image in the right upper corner ($\mathbf{B} = [011]_m \equiv [101]_o$).

The period doubling along $[010]_m \equiv [001]_o$ revealed by the HR image recorded along the pseudo-hexagonal zone axis (Fig. 3 f) can also be reproduced by the simulation program using the $P2_1/c$ space group. Fig. 9 shows a computed HR pattern along this zone axis for a thickness $t = 20$ *nm* and a defocus $df = -15$ *nm*. There is an obvious intensity variation between consecutive rows of white dots along $[010]_m \equiv [001]_o$.

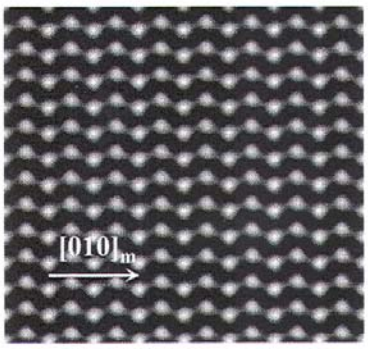

Fig. 9. Simulated HR contrast for $\mathbf{B} = [102]_m \equiv [210]_o$, a thickness t = 20 nm and a defocussing df = -15 nm.

Furthermore, measuring carefully the angle between the main crystallographic directions, $[100]_m \equiv [010]_o$ and $[001]_m \equiv [100]_o$, on the SAED and HR patterns corresponding to $\mathbf{B} = [100]_m \equiv [010]_o$ zone axis (Figs. 3 b and e), one can see that this is slightly different from 90°, being in fact 90.3°.

4. Conclusions

In this work we have studied the morphological and structural properties of a LYCMO thin film deposited by PLD on a Si <100> wafer previously coated with an MgO buffer layer. The MgO thin film has been deposited by PLD, also. Films are polycrystalline and show a columnar growth. By corroborating SAED and HRTEM studies, we have shown that the orthorhombic *Pnma* space group cannot correctly describe the crystalline structure of this material. We have seen that SAED patterns corresponding to main zone axes show diffraction spots in forbidden positions. On the other hand the corresponding experimental HRTEM images cannot be reproduced by the image simulation programs. A slightly distorted monoclinic lattice cell described by the $P2_1/c$ space group seems much more appropriated to characterize the perovskitic manganites because this space group allows for the presence of otherwise forbidden diffraction spots and permits also the HRTEM images to be reproduced by image simulation.

References

[1] S. Jin, H. M. O'Bryan, T. H. Tiefel, M. McCormack, W. W. Rhodes, Appl. Phys. Lett., **66**, 382 (1994).
[2] C. Zener, Phys. Rev., **82**, 403 (1951).
[3] A. Gupta, G. Q. Gong, G. Xiao, P. R. Duncombe, P. Lecoeur, P. Trouilloud, Y. Y. Wang, V. P. Dravid, J. Z. Sun, Phys. Rev., **B54**, R15629 (1996).
[4] O. I. Lebedev, G. Van Tendeloo, S. Amelinckx, B. Leibold, H.-U. Habermeier, Phys. Rev., **B58**, 8065 (1998).
[5] T. Y. Koo, S. H. Park, K.-B. Lee, Y. H. Jeong, Appl. Phys. Lett., **71**, 977 (1997).
[6] Z. Li, X. T. Zeng, H. K. Wong, J. Appl. Phys., **79**, 5188 (1996).
[7] R. Mahendiran, R. Mahesh, A. K. Raychaudhuri, C. N. R. Rao, Solid State Commun., **94**, 515 (1995).
[8] T. Y. Koo, S. H. Park, K.-B. Lee, Y. H. Jeong, Appl. Phys. Lett., **71**, 977 (1997).
[9] B. W. Chung, E. L. Brosha, F. H. Garzon, I. D. Raistrick, R. J. Houlton, M. E. Hawley, J. Mater. Res., **10**, 2518 (1995).
[10] V. S. Teodorescu, L. C. Nistor, M. Valeanu, C. Ghica, C. Sandu, I. N. Mihailescu, C. Ristoscu, J. P. Deville, J. Werckmann, J. Magn. & Magn. Mat., (in press).
[11] M. Hervieu, G. Van Tendeloo, V. Caignaert, A. Maignan, B. Raveau, Phys. Rev., **B53**, 14274 (1996).
[12] H. W. Zandbergen, J. Jansen, Ultramicroscopy, **80**, 59-68 (1999).
[13] J. Benedict, R. Anderson, S. J. Klepeis, Mat. Res. Soc. Symp. Proc., **254**, 121 (1992).